scientific reports

OPEN

Mixed convective flow of CNTs nanofluid subject to varying viscosity and reactions

Zakir Hussain[1]✉, Tasawar Hayat[2,3], Ahmed Alsaedi[3] & Muhammad Shoaib Anwar[4]

The addressed work explains SWCNTs (Single walled carbon nanotubnes) and MWCNTs (Multi walled carbon nanotubnes) nanofluid flow under the influences of temperature dependent viscosity and mixed convection. Comparative study of SWCNTs and MWCNTs suspended in base liquid is presented. Further heat and mass transfer are addressed for nanofluid effected by radiation, heat generation/ absorption and diffusion species. Mathematical development of problem is taken in cylindrical coordinates. System of highly nonlinear differential equations are constructed via appropriate transformations. The system of equations are tackled numerically by bvp4c MATLAB solver. The findings of the study show that larger volume fraction (ϕ) contributes to enhance the nanoliquid flow. The velocity by submerging MWCNTs is noted higher than SWCNTs. Furthermore, the relationship between the viscosity variable (θ_r) and the temperature is such that the temperature near the surface decreases with increase in (θ_r), while at the same time the temperature away from the surface increases. Subsequently, higher temperature is observed in SWCNTs-liquid compared to the MWCNTs-liquid to the similar values of (θ_r). Further, heat transfer is an increasing function of varying viscosity variable (θ_r).

The challenges and demands of advanced industries have been attracted the attention of researchers. The solar collectors used in devices are mostly affected by poor conductivity and low heat up capability of ordinary liquids. Choi[1] was the first one to take lead to enhance thermal conductivity in this way by mixing nano-sized particles in ordinary liquids. Nanoliquids are composed by suspension of chemical stable nano-scaled materials namely oxides, metals and carbides etc in base liquids. These novel fluids are termed as nanoliquids which enhance thermal characteristics of base liquids (engine oil, water, glycol etc). Ordinary liquids namely engine oil, water, glycol etc having low conductivity. Suspension of nanoparticles in low thermal conductivity liquids advance the thermal conductivity and hence accelerates the performance of industrial liquids. Entropy analysis on nanoliquid flow is discussed by Meshal et al.[2]. Shah et al.[3] studied flow of hybrid nanoliquid under the influence of magnetic field. Anwar et al.[4] addressed characteristics of shape factor for heat transfer in hybrid nanolqiuid. Melting effect on bio-convectional nanoliquid flow with second order slip has been analyzed by Waqas et al.[5]. Shah et al.[6] reported thermophoresis and brownian motion effects on CNTs flow. Aspects of Casson nanomaterial on Darcy-Forhheimer flow is studied by Islam et al.[7]. Optimal thermal characteristics of MHD nanoliquid flow in variable thickness channel has been documented by Zeeshan et al.[8]. Zeeshan et al.[9] has analyzed heat and mass transfer of MHD nanoliquid flow under the influences of radiation, viscous dissipation and Joule heating. Further studies of nanofluids are cited therein[10–12]. Khan et al.[13] addressed MHD nanoliquid with entropy generation in rotating frame. Sohail et al.[14] investigated Darcy Forchheimer hybrid nanoliquid in porous medium under the impact of entropy analysis. Khan et al.[15] analyzed non-axisymmetric Homann stagnation point nanofluid flow through multiple solutions. Huda et al.[16] elaborated Cattaneo–Christov model for nanofluid with moving needle. Reactive stretched flow of $Al_2O_3 - water$ in porous space is examined by Lia et al.[17].

Magnetic field application in fluid flow analysis has gained attention of scientists due to its wide range of utilization in many fields namely industries, drug delivery, MHD (Magnetohydrodynamics) generator, mechanical and physiological phenomena and many others. Nadeem et al.[18] studied MHD nanoliquid flow numerically. Malvandi et al.[19] studied mixed convection of MHD nanofluid saturate in vertical annulus. Activation energy in MHD squeezed flow with binary chemical reactions was studied by Ahmad et al.[20]. Hayat et al.[21] investigated

[1]Department of Mathematics, University of Baltistan, Skardu 16100, Pakistan. [2]Department of Mathematics, Quaid-I-Azam University 45320, Islamabad 44000, Pakistan. [3]Nonlinear Analysis and Applied Mathematics (NAAM) Research Group, Department of Mathematics, Faculty of Science, King Abdulaziz University, P.O. Box 80257, Jeddah 21589, Saudi Arabia. [4]Department of Mathematics, University of Jhang, Gojra Road, Jhang 35200, Pakistan. ✉email: zakir.qamar@yahoo.com

magnetohydrodynamics third grade nanoliquid convective flow by nonlinear stretched plate. Partial slip in MHD nanoliquid flow with viscous dissipation near stagnation point was investigated by Emad et al.[22].

Radiation does not need any medium to transmit. It depends on shape, temperature and propagates by electromagnetic waves. It is practiced that system in industries having little temperature difference in fluid caused problems. To overcome this difficulty the researchers incorporated a term named as radiation parameter. The variation in temperature of fluid and wall can be novel by this parameter. Cortell[23] summarized influence of heat generation and radiation in convective flow. Radiative MHD nanoliquid flow with convective condition has been discussed by Nadeem et al.[24]. Mohammadein et al.[25] studied influence of thermal radiation on MHD nanoliquid flow with suction/injection. Effect of heat source and radiation on MHD CNTs liquid flow in rotating frame is studied by Muhammad et al.[26]. Hayat et al.[27] explored non-Darcy flow of CNTs liquid subject to radiation and heat source.

Chemical reactions are categorized mainly in two types namely homogeneous and heterogeneous reactions. Reactions which encounter catalyst in same phase (namely gases, liquids, solids) correspond to homogeneous and reactions which happen in two or several different phases (like solid and gas, solid and liquid) as heterogeneous reactions. Some utilization of chemical reactions are found in iron oxidation, polymer and metallurgical industries. Reactions species have composite link for formation and usage of reactant species. Generally reactions rate depend on the magnitude of mass itself. A simple isothermal model proposed by Merkin et al.[28] investigates homogeneous-heterogeneous reactions in flow. Influence of chemical reaction in liquid flow was studied by Bhattacharyya[29]. Chemical reactive fluid flow was reported by Rashidi et al.[30] to explore mixed convection for heat and mass transfer. Convective flow with homogeneous-heterogeneous reactions saturated a porous medium was analyzed by Hayat et al.[31]. Zakir et al.[32] studied CNTs in flow of liquid by stretched cylinder with Darcy–Forhheimer effect.

This work aims to address the analysis specifically in six dimensions. First of these is the formulation of problem, computation and then associated analysis. Secondly the comparative analysis of CNTs liquid under the influence of applied magnetic field. An induced magnetic field has been neglected for low Reynolds number. Third to study the effects of temperature dependent viscosity, viscous dissipation and Joule heating. Fourthly to examine the mixed convection and magnetohydrodynamics on CNTs liquid flow. Fifth heat transfer has been explored via thermal radiation and heat source/sink. Sixth mechanism of homogeneous and heterogeneous reactions are disclosed.

The current study contributes mathematical modeling, computation and comparison of associated analysis. To the best of authors' knowledge, no one has attempted comparative study of SWCNTs-liquid and MWCNTs-liquid under the influences of magnetohydrodynamics, mixed convection, temperature dependent viscosity, thermal radiation, heat source sink/sink, viscous dissipation and Joule heating and homogeneous–heterogeneous reactions. This analysis is a new contribution in this dimension.

Water is treated as a base fluid for the submerging particles namely multi walled and single walled nanotubes. Water and nanomaterials are considered thermally balanced. The problem formulation has been carried out in cylindrical coordinates. System of nonlinear differential equations are changed to nonlinear ordinary differential equation via suitable transformations. Effects of various variables on velocity, temperature, skin friction and Nusselt number have been studied through graphical and tabulated outcomes.

CNTs namely SWCNTs and MWCNTs are seamless cylinders containing at least one layer of graphene (SWCNTs or MWCNTs) having closed or open ends. CVD (chemical vapor deposition) is the strong production of high CNTs volume mode that normally utilizes fluidized bed-reactors which strengthen diffusion of uniform gases and heat transport to metal catalyst nanomaterials. For this understanding, CNTs nanoliquid flow with varying viscosity of base liquid is one of the interesting discussion under consideration.

Problem development

In this analysis, it is considered that two-dimensional incompressible mixed convective flow of CNTs nanoliquid by stretchable cylinder. The liquid flow is caused by stretching cylinder. The viscosity of base liquid varies with the variation of temperature. Base liquid contains homogeneous combination of CNTs particles. Further more, CNTs particles and base liquid are in thermal equilibrium. Linearly stretching cylinder (i.e. $w_e = \frac{U_0 z}{l}$) is along axial direction ($z - axis$) while liquid is assumed to deform in radial direction ($r - axis$). Figure 1 addresses the geometric configuration of flow problem. Heat transfer characteristics are explored via heat generation/absorption, viscous dissipation and Joule heating. Diffusion species are accounted in base liquid for reactions.

The fluid viscosity[33] is treated inversely linear function of temperature i.e.,

$$\begin{cases} \frac{1}{\mu(T)} = \frac{1}{\mu_\infty}(1 + \gamma_0(T - T_\infty)) = \frac{\gamma_0}{\mu_\infty}(T - T_r) = a_1(T - T_r) = \frac{1}{\mu_\infty}\left(\frac{\theta_r - \theta}{\theta_r}\right), \\ \mu(T) = \mu_\infty\left(\frac{\theta_r}{\theta_r - \theta}\right), \end{cases} \quad (1)$$

here

$$\left\{ T_r = \left(T_\infty - \frac{1}{\gamma_0}\right), \gamma_0 = \left(\frac{1}{T_\infty - T_r}\right), \theta_r = \left(\frac{T_r - T_\infty}{T_w - T_\infty}\right) = \left(\frac{1}{\gamma_0(T_w - T_\infty)}\right), a_1 = \left(\frac{\gamma_0}{\mu_\infty}\right), \right.$$

where the constants (T_r) and (a_1) depend on the initial state and thermal characteristics (γ_0) of the liquid. It is often scaled that ($a_1 > 0$) and ($a_1 < 0$) for liquids and gases respectively. The values of (θ_r) is computed by viscosity of liquid under consideration and the difference of operating temperature. Larger (θ_r) corresponds to smaller (γ_0) or ($T_w - T_\infty$). Thus the influence of varying viscosity can be ignored while the smaller (θ_r) tends to
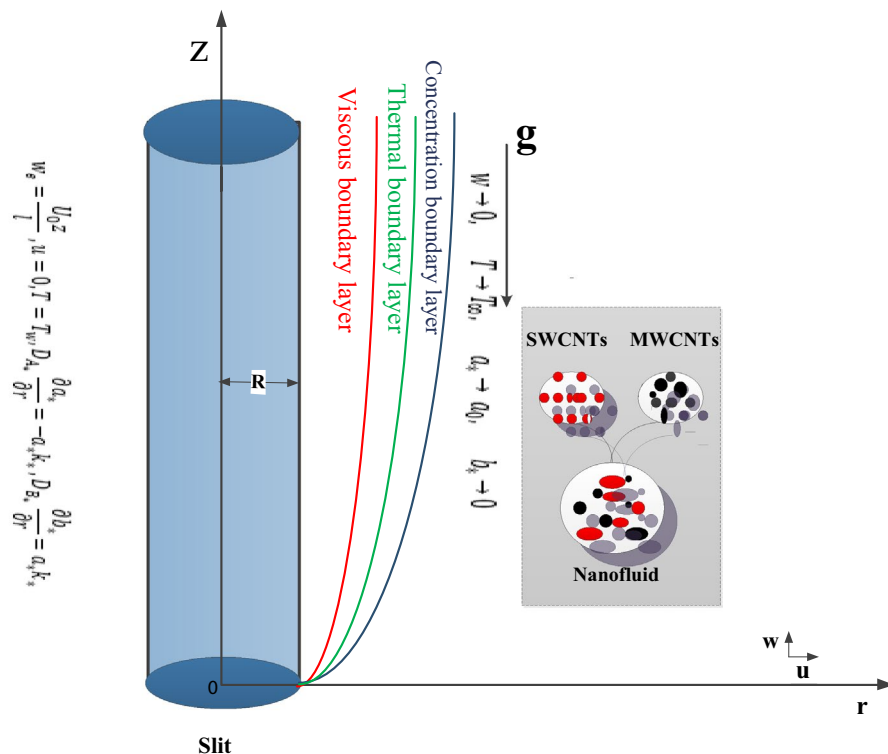
Figure 1. Schematic representation of problem.

either the liquid viscosity changes remarkably or high difference of operating temperature. The varying viscosity changes to constant ($\mu = \mu_\infty$) for $\theta_r - > \infty$ (i.e. $\gamma_0 - > 0$).

For heterogeneous-homogeneous reactions, the model of isothermal[28] is defined by

$$\mathbf{A}_\star + 2\mathbf{B}_\star \rightarrow 3\mathbf{B}_\star, rate = k_p a_\star b_\star^2. \tag{2}$$

At surface of catalyst the first-order reaction is

$$\mathbf{A}_\star \rightarrow \mathbf{B}_\star, rate = k_\star a_\star. \tag{3}$$

Where ($a_\star$, $b_\star$) stand for concentrations of species ($\mathbf{A}_\star$, $\mathbf{B}_\star$), (k_p, $k_\star$) show the rate constants. The auto-catalyst ($\mathbf{B}_\star$) is taken inside the boundary layer and outside it is dealt equal concentration (a_0) of reactant ($\mathbf{A}_\star$). Equation (3) reveals that there is no reaction rate outside the boundary layer.

The governing problems via boundary layer approximation in cylindrical coordinates are as follows[28,34]:

$$\frac{\partial(ru)}{\partial r} + \frac{\partial(rw)}{\partial z} = 0, \tag{4}$$

$$w\frac{\partial w}{\partial z} + u\frac{\partial w}{\partial r} = \frac{1}{\rho_{nf}}\left(\frac{\partial \mu_{nf}(T)}{\partial r}\frac{\partial w}{\partial r} + \frac{1}{r}\mu_{nf}(T)\frac{\partial w}{\partial r} + \mu_{nf}(T)\frac{\partial^2 w}{\partial r^2}\right) \\ + gB(T - T_\infty) - \frac{\sigma_{nf}}{\rho_{nf}}B_0^2 w, \tag{5}$$

$$u\frac{\partial T}{\partial r} + w\frac{\partial T}{\partial z} = \frac{k_{nf}}{(C_p\rho)_{nf}}\left(\frac{\partial^2 T}{\partial r^2} + \frac{1}{r}\frac{\partial T}{\partial r}\right) + \frac{16\sigma^\star T_0^3}{3k^\star(C_p\rho)_{nf}}\left(\frac{\partial^2 T}{\partial r^2} + \frac{1}{r}\frac{\partial T}{\partial r}\right) \\ + \frac{\mu_{nf}(T)}{(C_p\rho)_{nf}}\left(\frac{\partial w}{\partial r}\right)^2 + \frac{Q_0(T - T_\infty)}{(C_p\rho)_{nf}}, \tag{6}$$

$$u\frac{\partial a_\star}{\partial r} + w\frac{\partial a_\star}{\partial z} = D_{A_\star}\left(\frac{\partial^2 a_\star}{\partial r^2} + \frac{\star}{r}\frac{\partial a_\star}{\partial r}\right) - k_p a_\star b_\star^2,$$

$$u\frac{\partial b_\star}{\partial r} + w\frac{\partial b_\star}{\partial z} = D_{B_\star}\left(\frac{\partial^2 b_\star}{\partial r^2} + \frac{1}{r}\frac{\partial b_\star}{\partial r}\right) + k_p a_\star b_\star^2,$$

(7)

with conditions

$$\begin{cases} w_e = \frac{U_0 z}{l}, & u = 0, & T = T_w, \\ D_{A_\star}\frac{\partial a_\star}{\partial r} = -a_\star k_\star, & D_{B_\star}\frac{\partial b_\star}{\partial r} = a_\star k_\star & at \quad r = R, \\ w \to 0, & T \to T_\infty, & a_\star \to a_0, \quad b_\star \to 0 \quad as \quad r \to \infty, \end{cases}$$

(8)

where (w, u) the velocity components, (ρ_{nf}) the density of nanoliquid, $((C_p)_{nf})$ the specific heat of nanoliquid, $(\mu_{nf}(T))$ the dynamic viscosity of nanomaterial, (k_{nf}) the thermal conductivity nanoliquid, (w_e) the stretching velocity, (U_0) the reference velocity, (l) the characteristics length, (R) the radius of cylinder, (B_0) the strength of magnetic field, $((\sigma)_{nf})$ electric transport of nanofluid, (g) the gravitational acceleration, (B) the thermal coefficient, $(Q_0(T - T_\infty))$ the heat generate per unit volume, (T_w, T_∞) the wall and ambient temperatures, $(\sigma^\star)$ the Stefan Boltzmann constant, $(k^\star)$ the mean absorption coefficient and $(D_{A_\star}, D_{B_\star})$ the diffusion coefficients ($\mathbf{A}_\star$, $\mathbf{B}_\star$) respectively.

Following models[35–37] one has

$$\mu_{nf} = \frac{\mu_f(T)}{(1-\phi)^{2.5}}, \quad \rho_{nf} = (1-\phi)\rho_f + \phi(\rho)_{CNT},$$

$$(C_p\rho)_{nf} = (1-\phi)(C_p\rho)_f + \phi(C_p\rho)_{CNT},$$

$$\frac{k_{nf}}{k_f} = \frac{(1-\phi) + 2\phi\frac{k_{CNT}}{k_{CNT}-k_f}\ln\frac{k_{CNT}+k_f}{2k_f}}{(1-\phi) + 2\phi\frac{k_f}{k_{CNT}-k_f}\ln\frac{k_{CNT}+k_f}{2k_f}},$$

$$\frac{\sigma_{nf}}{\sigma_f} = \frac{3(\sigma-1)\phi}{(\sigma+2)-(\sigma-1)\phi} + 1, \quad \sigma = \frac{\sigma_{CNT}}{\sigma_f},$$

(9)

in which (ϕ) denotes the volume fraction of nanosized particle, $(\rho)_f$ the base liquid density, $(\mu)_f$ the dynamic viscosity of base liquid, $(\rho)_{CNT}$ the density of nanotubes, $(k)_f$ the base liquid conductivity, $(k)_{CNT}$ represents nanotubes thermal conductivity, $(\sigma)_{CNT}$ and $(\sigma)_f$ the electric conductivity of base liquid and nanoparticle respectively.

Letting

$$\eta = \sqrt{\frac{U_0}{(\nu_\infty)_f l}}\left(\frac{r^2 - R^2}{2R}\right), \quad \psi = \sqrt{w_e(\nu_\infty)_f z}Rf(\eta) \quad w = \frac{U_0 z}{l}f'(\eta),$$

$$u = -\sqrt{\frac{(\nu_\infty)_f U_0}{l}}\frac{R}{r}f(\eta), \quad \theta(\eta) = \frac{T - T_\infty}{T_w - T_\infty}, \quad \Phi_\star(\eta) = \frac{a_\star}{a_0}, \quad h_\star(\eta) = \frac{b_\star}{a_0}.$$

(10)

Equation (4) is trivially confirmed and Eqs. (5 – 8) reduce to

$$(1 + 2\gamma\eta)f''' + 2\gamma f'' - \left(\frac{1}{\theta_r - \theta}\right)(1 + 2\gamma\eta)\theta'f''$$

$$+ \left(\frac{\theta_r - \theta}{\theta_r}\right)(1-\phi)^{2.5}\left(1 - \phi + \phi\frac{(\rho)_{CNT}}{(\rho)_f}\right)(ff'' - (f')^2)$$

$$+ \left(\frac{\theta_r - \theta}{\theta_r}\right)(1-\phi)^{2.5}\left(1 - \phi + \phi\frac{(C_p\rho)_{CNT}}{(C_p\rho)_f}\right)Gr\theta$$

$$- \left(\frac{\theta_r - \theta}{\theta_r}\right)(1-\phi)^{2.5}\left(\frac{3(\sigma-1)\phi}{(\sigma+2)-(\sigma-1)\phi} + 1\right)M_f f' = 0,$$

(11)

$$\left(\frac{(k)_{nf}}{(k)_f} + \frac{4}{3}R_d\right)\left((1 + 2\gamma\eta)\theta'' + 2\gamma\theta'\right) + Pr\left(Q_r\theta + \frac{(C_p\rho)_{nf}}{(C_p\rho)_f}f\theta'\right)$$

$$+ Pr(1-\phi)^{2.5}\left(\frac{\theta_r}{\theta_r - \theta}\right)Ec(1 + 2\gamma\eta)(f'')^2 = 0,$$

(12)

$$\frac{1}{Sc}\left((1 + 2\gamma\eta)\Phi_\star'' + \gamma\Phi_\star'\right) + f\Phi_\star' - K\Phi_\star h_\star^2 = 0,$$

(13)

$$\frac{\delta_\star}{Sc}\left((1 + 2\gamma\eta)h_\star'' + \gamma h_\star'\right) + fh_\star' + K\zeta_\star h_\star^2 = 0,$$

(14)

	Base fluid	Nanoparticles	
Physical properties	**Water**	**SWCNTs**	**MWCNTs**
ρ (kg/m^3)	997	2600	1600
C_p (J/kgK)	4179	425	796
k (W/mK)	0.613	6600	3000
σ (S/m)	0.005	1×10^7	1×10^7
Pr	6.2	–	–

Table 1. Thermophysical characteristics of CNTs liquid[10,36]. Where (ρ, C_p, k, σ) the density, specific heat, thermal conductivity and electric conductivity respectively.

with

$$f(0) = 0, \quad f'(0) = 1, \quad \theta(0) = 1, \quad \Phi'_\star(0) = Ks\Phi_\star(0), \quad \delta_\star h'(0) = -Ks\Phi_\star(0),$$
$$f'(\eta) = 0, \quad \theta(\eta) = 0, , \quad \Phi_\star(\eta) \to 1, \quad h_\star(\eta) \to 0, \quad as \quad \eta \to \infty, \tag{15}$$

where $\left(\gamma = \frac{1}{R}\sqrt{\frac{(v_\infty)_f l}{U_0}}\right)$ depicts the curvature parameter, $\left(Gr = \frac{\lambda_1}{Re_z^2}\right)$ the mixed convection variable, $\left(Re_z = \frac{w_e z}{(v_\infty)_f}\right)$ the local Reynolds number, $\left(\lambda_1 = \frac{g(T_w - T_\infty)Bz^3}{(v_\infty)_f^2}\right)$ local Grashof number, $\left(M_f = \frac{\beta_0^2 \sigma_f l}{(\rho_\infty)_f U_0}\right)$ the Hartman number, $\left(Ec = \frac{w_e^2}{(C_p)_f(T_\infty - T_w)}\right)$ the Eckert number, $\left(R_d = \frac{4\sigma^\star T_0^3}{3k^\star k_f}\right)$ the radiation parameter, $\left(Q_r = \frac{Q_0 l}{U_0(\rho_\infty C_p)_f}\right)$ the heat generation/absorption parameter, $\left(K = \frac{k_p a_0^2 l}{U_0}\right)$ the homogeneous variable, $\left(Ks = \frac{k_\star}{D_{A_\star}}\sqrt{\frac{(v_\infty)_f l}{U_0}}\right)$ the heterogeneous variable, $\left(Sc = \frac{(v_\infty)_f}{D_{A_\star}}\right)$ the Schmidt number, $Pr = \frac{(\mu_\infty C_p)_f}{k_f}$ and $\left(\delta_\star = \frac{D_{B_\star}}{D_{A_\star}}\right)$ the diffusion ratio coefficient. The Prandtl and Schmidt numbers have been kept constant throughout the study.

One has, for equal diffusion coefficients $D_{A_\star}$ and $D_{B_\star}$ as[28];

$$\Phi_\star(\eta) + h_\star(\eta) = 1.$$

Equations (13)–(14) imply that

$$(1 + 2\gamma\eta)\Phi''_\star + 2\gamma\Phi'_\star + Scf\Phi'_\star - ScK\Phi_\star(1 - \Phi_\star)^2 = 0. \tag{16}$$

$$\Phi'_\star(0) = Ks\Phi_\star(0), \quad \Phi_\star(\eta) \to 1 \quad as \quad \eta \to \infty. \tag{17}$$

Skin friction coefficient and Nusselt number are

$$C_f = \frac{\tau_w}{\frac{\rho U_0^2 z^2}{2l^2}}, \qquad Nu_z = \frac{zq_w}{k_f(T_w - T_\infty)}, \tag{18}$$

where τ_w and q_w are defined as;

$$\begin{cases} \tau_w = -\mu_f\left(\frac{\partial w}{\partial r}\right)_{r=R}, & q_w = -\left(k_{nf} + \frac{16\sigma^\star T_0^3}{3k^\star}\right)\left(\frac{\partial T}{\partial r}\right)_{r=R}, \\ C_f Re_z^{\frac{1}{2}} = -\frac{1}{(1-\phi)^{2.5}}f''(0), & Nu_z Re_z^{-\frac{1}{2}} = -\left(\frac{k_{nf}}{k_f} + \frac{4}{3}R_d\right)\theta'(0), \end{cases} \tag{19}$$

where $Re_z^{\frac{1}{2}} = \sqrt{\frac{U_0}{(v_\infty)_f l}}z$ represents the local Reynolds number.

Discussion

This section elaborates the graphical discussion for SWCNTs and MWCNTs nanofluids. SWCNTs is indicated by the solid lines while MWCNTs by dashed lines. The values Curvature variable (γ) = Hartman number (M_f) = Mixed convection (Gr) = Volume fraction (ϕ) = Radiation parameter (R_d) = Variable viscosity parameter (θ_r) = Eckert number (Ec) = 0.1, Prandtl number $(Pr = 6.2)$, Homogeneous reaction variable $(K = 0.7)$, Heterogeneous reaction variable $(Ks = 0.9)$ and Schmidt number $(Sc = 1.2)$ are taken for outcomes. Further the values of variables are taken constant except the specific variable considered in Figures. The thermophysical characteristics of CNTs nanoliquid is defined in Table 1. In Table 1, $(\rho, C_p, k)^{10}$ denote the density, the specific heat and the thermal conductivity while $(\sigma)^{36}$ represents the electric conductivity. The outcomes of curvature, Hartman number, Grashof number, volume fraction and others involved dimensionless variables are elaborated for the distributions, velocity $(f'(\eta))$, temperature $(\theta(\eta))$, concentration $(\Phi(\eta))$, Skin friction coefficient $\left(C_f Re_z^{\frac{1}{2}}\right)$, Nusselt number $\left(Nu_z Re_z^{-\frac{1}{2}}\right)$.

5
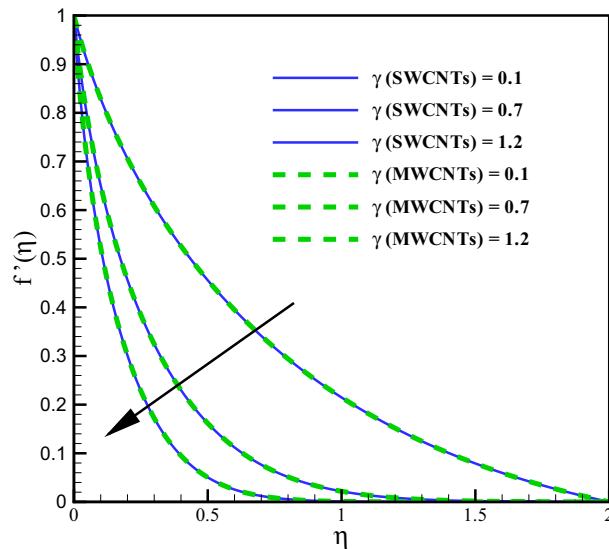
Figure 2. Curves via γ for $f'(\eta)$.
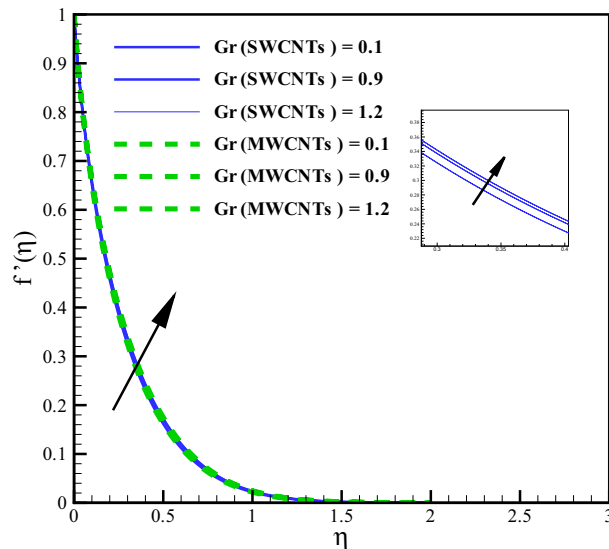
Figure 3. Curves via Gr for $f'(\eta)$.

Velocity profile. Larger curvature variable (γ) declines the velocity distribution (see Fig. 2). Clearly (γ) and (R) inversely relate to each other and therefore, the resistive force enhances for the nanoliquid flow. The velocity profile thus declines. Figure 3 is sketched to discuss the effect of mixed convection variable (Gr) on velocity field. From the figure, it is observed that velocity enhances for both SWCNTs and MWCNTs. Because the mixed convection variable directly relates to thermal buoyancy forces and the resistive force becomes less against larger (Gr). Consequently, the velocity profile increases. Figure 4 shows curves of Hartman number (M_f) for velocity. The flow field declines for larger (M_f). Lorentz force rises for higher (M_f) and thus the velocity of liquid decreases. The velocity fields for SWCNTs and MWCNTs behaves similarly against (γ), (Gr) and (M_f). Impact of volume fraction for SWCTs-water and MWCNTs-water is addressed in Fig. 5. Nanoliquid flow boosts when the values of (ϕ) increase. Physically, larger (ϕ) caused more convective flow that enhances the liquid velocity. Furthermore, the flow by submerging MWCNTs nanomaterial is observed higher than by adding SWCNTs nanoparticles. Because the density of MWCNTs is lighter when compared to SWCNTs density.

Temperature profile. The curves for temperature against heat generation variable (Q_r) has been presented in Fig. 6. Thermal layer enhances via larger (Q_r). Heat transfer increases against larger (Q_r) due to the direct relation with thermal constant coefficient. Temperature variations is noted similar for both type CNTs. The temperature curves follow free stream condition for larger η. Figure 7 addresses the influence of viscous dissipation (i.e. Eckert number (Ec)) on temperature. The temperature rises when (Ec) is increased. Larger Ec leads to

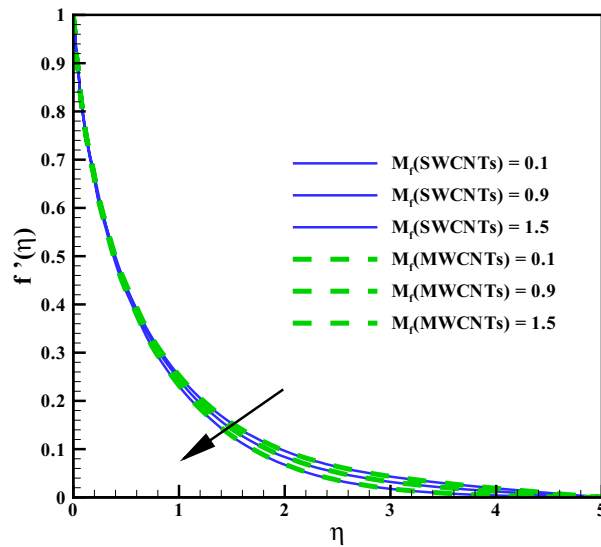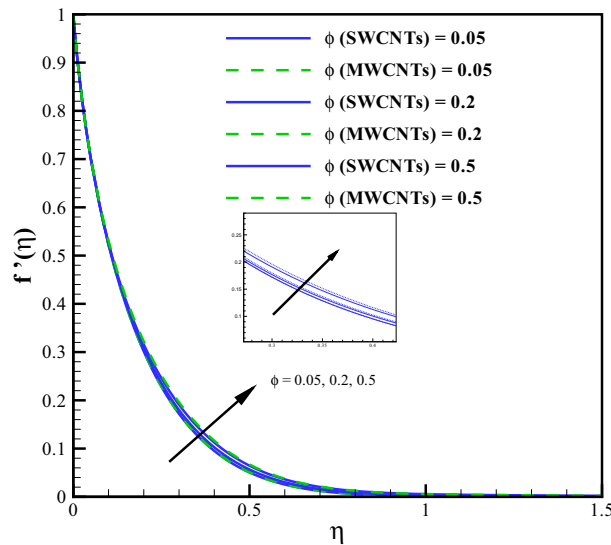**Figure 4.** Curves via M_f for $f'(\eta)$.

**Figure 5.** Curves via ϕ for $f'(\eta)$.

higher the kinetic energy of liquid molecules resulting more collision between liquid molecules. Consequently heat produce, due to collisions and the temperature rises significantly. Moreover, same temperature behavior is noted for cylinder shaped SWCNTs and MWCNTs nanofluids. Figure 8 shows the effect of curvature variable on temperature. The fluid heats up by increasing (γ). Higher values of curvature variable reduce the radius of stretchable cylinder. Subsequently heat produce due to friction that enhances the temperature for the nanoliquid. Moreover, the temperature of liquid is noted higher by addition of MWCNTs nanomaterials than SWCNTs nanomaterials. The curves of radiation variable (R_d) for $(\theta(\eta))$ is shown in Fig. 9. Outcomes of radiation variable results enhancement in temperature $(\theta(\eta))$. Higher values of radiation variable results increase in heat flux at the surface. Hence, the thermal layer thickness increases. Figure 10 is sketched for the temperature dependent viscosity variable on temperature field. Figure shows that increment in (θ_r), contributes first declines and than enhances the temperature. Physically, it reflects that smaller (θ_r) tends to remarkable change in viscosity or the higher the difference of operating temperature. However, opposite trend is noted for larger (θ_r). Hence the temperature first declines and than enhances. The temperature is noted higher for SWCNTs near the surface than MWCNTS while the temperature is observed higher far away from the surface when compared with SWCNTs.

Concentration profile. Figure 11 addresses the concentration profile via larger curvature variable (γ). The Concentration profile enhances against (γ). Physically, the resistive forces produce between liquid molecules for larger (γ) due to inverse relation with radius of cylinder. Figure 12 shows the curves for concentration gradient
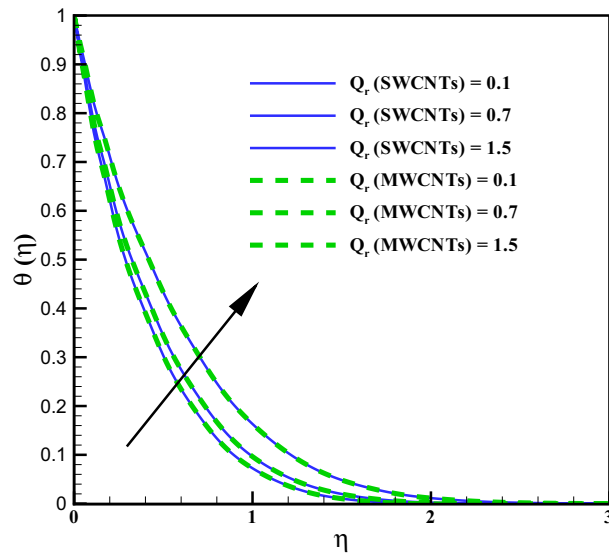
Figure 6. Curves via Q_r for $\theta(\eta)$.
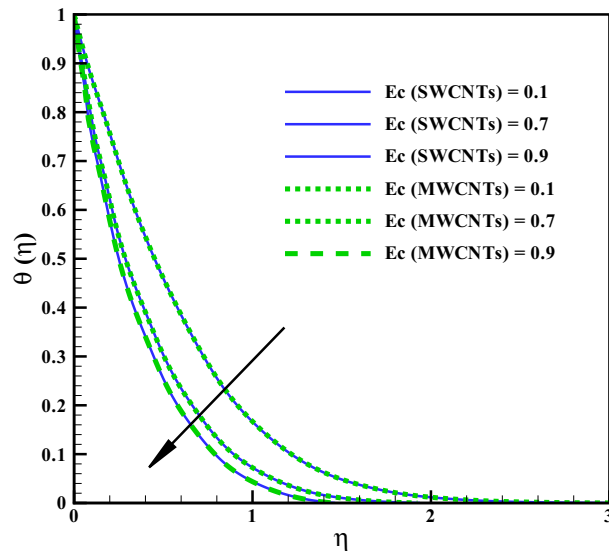

Figure 7. Curves via Ec for $\theta(\eta)$.

via homogeneous variable (K). The solutat layer thickness increases for larger (K). In fact, there is direct relation between chemical reaction and the values of (K). The concentration for larger heterogeneous variable (Ks) can be seen in Fig. 13. Same behavior is noted against (Ks). Figure 14 shows the behavior of skin friction coefficients via (M_f) and (ϕ). Skin friction enhances for larges values of (M_f) and (ϕ). Resistive forces develop by addition of volume fraction and larger Hartman number. Figure 15 addresses the Nusselt number via variables (R_d) and (Q_r). Nusselt number increases for larger Q_r and it decreases for R_d. Larger (Q_r) results small changes in viscosity or difference of operating temperature. Thus, heat transfer at the surface enhances. Nusselt number for (γ) and (Q_r) is opposite (see Fig. 16). The skin friction can be controlled via (M_f) and (ϕ). Heat transfer rate at surface advances for larger (Q_r) and smaller (R_d) and (γ).

Main findings
After studying the governing problem via stretchable cylinder, the key results have been mentioned below:

1. The velocity fields decrease against curvature (γ) and Hartman (M_f) variables and increase for larger volume fraction (ϕ) and mixed convection (Gr) variable. Furthermore same behavior is observed for SWCNTs and MWCNTs against Hartman, mixed convection and curvature variables. In addition, the velocity profile for MWCNTs nanofluid is noted higher than SWCNTs nanofluid against (ϕ).
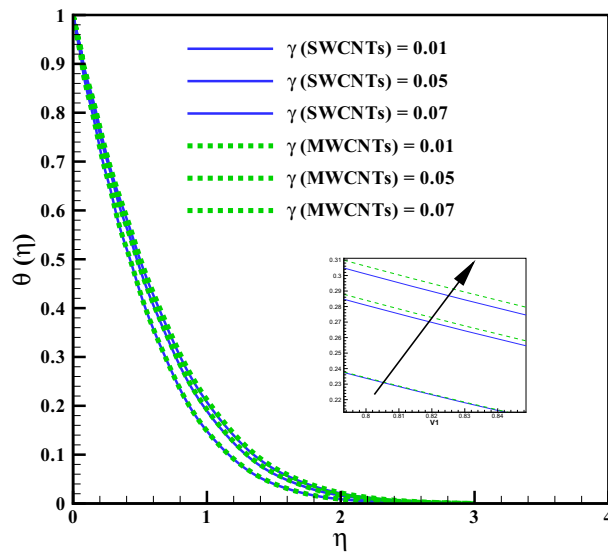
Figure 8. Curves via γ for $\theta(\eta)$.
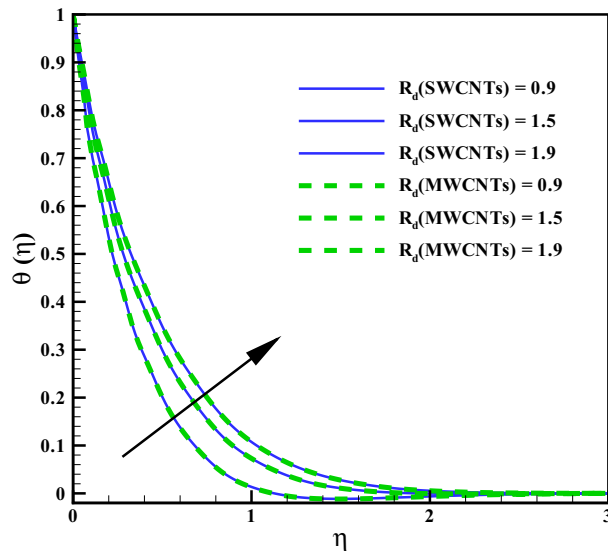
Figure 9. Curves via R_d for $\theta(\eta)$.

2. Temperature is an increasing function of curvature variable (γ) while for viscosity variable (θ_r), the temperature decreases close to the surface and than increases far way from the surface. In addition, temperature in case of SWCNTs nanomaterials is observed higher when compared with MWCNTs nanomaterials against curvature and viscosity variables. Similar trend is observed for SWCNTs and MWCNTs against Eckert, Heat generation, mixed convection and Radiation variables.

3. The solutal layer thickness decreases against curvature variable (γ) while opposite behavior has been seen against homogeneous-heterogeneous reactions variables (K, Ks).

4. Skin friction coefficient develops for (M_f) and it declines for larger (ϕ). Nusselt number ($Nu_z Re_z^{\frac{-1}{2}}$) boosts against (θ_r) and it decreases via radiation and curvature variables.

The findings of current analysis have its usage in many phenomena like extrusion where the submerging particles to the liquid for cooling purpose under a certain temperature, wire drawing, condensation processes of metallic plate in bath and cooling glasses etc. It could help to develop catalytic phenomenon demanding the species reactions for the scientific community.
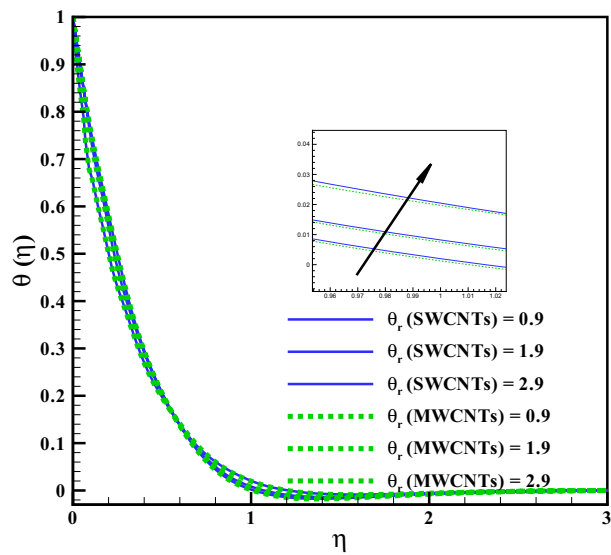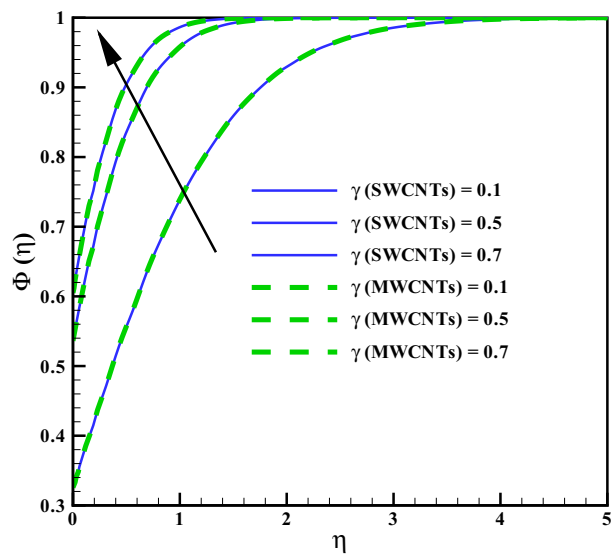
Figure 10. Curves via θ_r for $\theta(\eta)$.
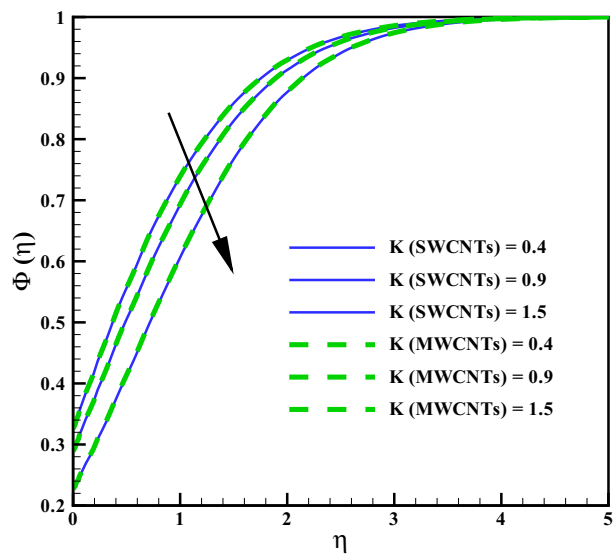

Figure 11. Curves via γ for $\Phi(\eta)$.

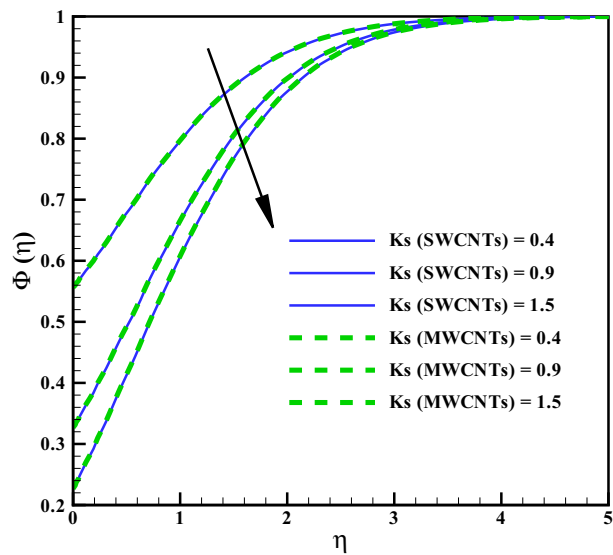**Figure 12.** Curves via K for $\Phi(\eta)$.

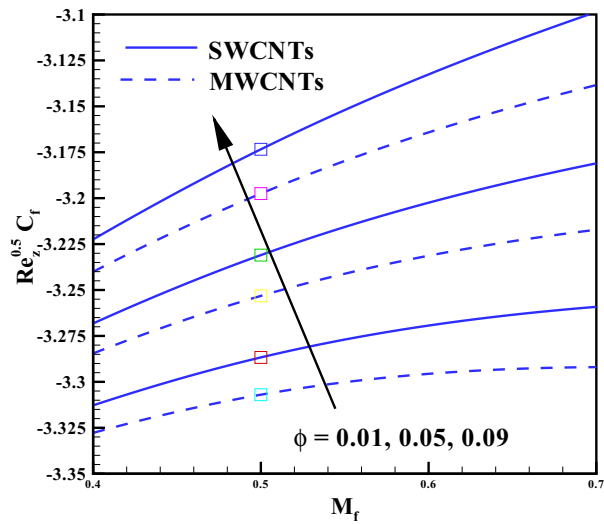**Figure 13.** Curves via Ks for $\Phi(\eta)$.

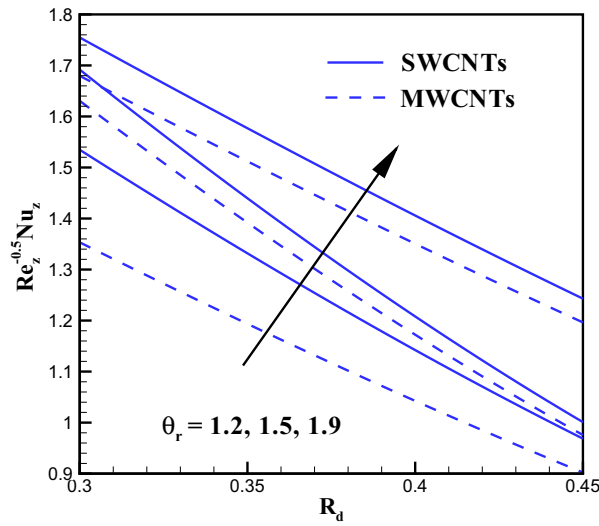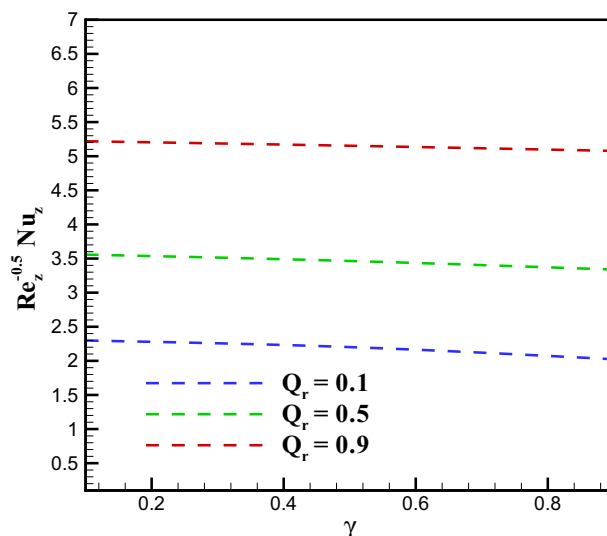**Figure 14.** Plots for $C_f Re_z^{\frac{1}{2}}$ via M_f and ϕ.

Figure 15. Plots for $Nu_z Re_z^{-0.5}$ via R_d and θ_r.

Figure 16. Plots for $Nu_z Re_z^{-0.5}$ via γ and Q_r.

References

1. Choi, S. U. S. Enhancing thermal conductivity of fluids with nanoparticles. In *Developments and Applications of Non-Newtonian Flows*, FED-Vol. 231/MD 66 (eds Siginer, D. A., Wang, H. P.) 99–105 (ASME, 1995).
2. Shutaywi, M. & Shah, Z. Mathematical modeling and numerical simulation for nanofluid flow with entropy optimization. *Case Stud. Therm. Eng.* **26**, 101198 (2021).
3. Shah, Z., Saeed, A., Khan, I., Selim, M. M. & Kumam, P. Numerical modeling on hybrid nanofluid (Fe3O4+ MWCNT/H2O) migration considering MHD effect over a porous cylinder. *PLoS ONE* **7**, e0251744 (2021).
4. Anwar, T., Kumam, P., Shah, Z. & Sitthithakerngkiet, K. Significance of shape factor in heat transfer performance of molybdenum-disulfide nanofluid in multiple flow situations. A comparative fractional study. *Molecules* **26**, 3711 (2021).
5. Waqas, H., Farooq, U., Shah, Z., Kumam, P. & Shutaywi, M. Second-order slip effect on bio-convectional viscoelastic nanofluid flow through a stretching cylinder with swimming microorganisms and melting phenomenon. *Sci. Rep.* **11**, 1–16 (2021).
6. Shah, Z., Dawar, A. & Islam, S. Influence of Brownian motion and thermophoresis parameters on silver-based Di-Hydrogen CNTs between two stretchable rotating disks. *Phys. Scr.* **96**, 055205 (2021).
7. Islam, S. *et al.* MHD Darcy–Forchheimer flow due to gyrotactic microorganisms of Casson nanoparticles over a stretched surface with convective boundary conditions. *Phys. Scr.* **96**, 015206 (2020).
8. Zeeshan, A., Pervaiz, Z., Shehzad, N., Nayak, M. K. & Al-Sulami, H. H. Optimal thermal performance of magneto-nanofluid flow in expanding/contracting channel. *J. Therm. Anal. Calorim.* **143**, 2189–2201 (2021).
9. Zeeshan, A., Majeed, A., Akram, M. J. & Alzahrani, F. Numerical investigation of MHD radiative heat and mass transfer of nanofluid flow towards a vertical wavy surface with viscous dissipation and Joule heating effects using Keller-box method. *Math. Comput. Simul.* **190**, 1080–1109 (2021).
10. Hayat, T., Hussain, Z., Alsaedi, A. & Asghar, S. Carbon nanotubes effects in the stagnation point flow towards a nonlinear stretching sheet with variable thickness. *Adv. Powder Technol.* **27**, 1677–1688 (2016).
11. Gireesha, B. J., Mahanthesh, B., Thammanna, G. T. & Sampathkumar, P. B. Hall effects on dusty nanofluid two-phase transient flow past a stretching sheet using KVL model. *J. Mol. Liq.* **256**, 139–147 (2018).
12. Pattnaik, P. K., Abbas, M. A., Mishra, S., Khan, S. U. & Bhatti, M. M. Free convective flow of Hamilton–Crosser model gold-water nanofluid through a channel with permeable moving walls. *Combin. Chem. High Throughput Screen.*https://doi.org/10.2174/1386207324666210813112323 *(2021)*.
13. Khan, M. I., Hafeez, M. U., Hayat, T., Khan, M. I. & Alsaedi, A. Magneto rotating flow of hybrid nanofluid with entropy generation. *Comput. Methods Program. Biomed.* **183**, 105093 (2020).
14. Khan, A. S., Khan, M. I., Hayat, T. & Alsaedi, A. Darcy–Forchheimer hybrid (MoS2, SiO2) nanofluid flow with entropy generation. *Comput. Methods Program. Biomed.* **185**, 105152 (2020).
15. Khan, A. U., Saleem, S., Nadeem, S. & Alderremy, A. A. Analysis of unsteady non-axisymmetric Homann stagnation point flow of nanofluid and possible existence of multiple solutions. Phys. A Stat. Mech. Appl. 123920 (2019).
16. Huda, N.U., Hamid, A., & Khan, M. Impact of Cattaneo–Christov model on Darcy–Forchheimer flow of ethylene glycol base fluid over a moving needle. J. Mater. Res. Tech. (in press).
17. Liu, C., Pan, M., Zheng, L. & Lin, P. Effects of heterogeneous catalysis in porous media on nanofluid-based reactions. *Int. Commun. Heat Mass Transf.* **110**, 104434 (2020).
18. Nadeem, S., Haq, R. U. & Khan, Z. H. Numerical study of MHD boundary layer flow of a Maxwell fluid past a stretching sheet in the presence of nanoparticles. *J. Taiwan Inst. Chem. Eng.* **45**, 121–126 (2014).
19. Malvandi, A., Safaei, M. R., Kaffash, M. H. & Ganji, D. D. MHD mixed convection in a vertical annulus filled with Al2O3-water nanofluid considering nanoparticle migration. *J. Magn. Magn Mater.* **382**, 296–306 (2015).
20. Ahmad, S., Farooq, M., Mir, N. A., Anjum, A. & Javed, M. Magneto-hydrodynamic flow of squeezed fluid with binary chemical reaction and activation energy. *J. Cent. South Univ.* **26**, 1362–1373 (2019).
21. Hayat, T., Riaz, R., Aziz, A. & Alsaedi, A. Influence of Arrhenius activation energy in MHD flow of third grade nanofluid over a nonlinear stretching surface with convective heat and mass conditions. Phys. A Stat. Mech. Appl. 124006 (2020).
22. Emad, A.H., & Pop, I. MHD flow and heat transfer near stagnation point over a stretching/shrinking surface with partial slip and viscous dissipation: Hybrid nanofluid versus nanofluid. Powder Technol. (in press).

23. Cortell, R. Internal heat generation and radiation effects on a certain free convection flow. *Int. J. Nonlinear Sci.* **9**, 468–479 (2010).
24. Nadeem, S. & Haq, R. U. Effect of thermal radiation for megnetohydrodynamic boundary layer flow of a nanofluid past a stretching sheet with convective boundary conditions. *J. Comput. Theor. Nanosci.* **11**, 32–40 (2014).
25. Mohammadein, S. A., Raslan, K., Abdel-Wahed, M. S. & Abedel-Aal, E. M. KKL-model of MHD CuO-nanofluid flow over a stagnation point stretching sheet with nonlinear thermal radiation and suction/injection. *Results Phy.* **10**, 194–199 (2018).
26. Muhammad, S., Ali, G., Shah, Z., Islam, S. & Hussain, S. A. The rotating flow of magneto hydrodynamic carbon nanotubes over a stretching sheet with the impact of non-linear thermal radiation and heat generation/absorption. *Appl. Sci.* **8**(4), 482 (2018).
27. Hayat, T., Ullah, S., Khan, M. I., Alsaedi, A. & Zia, Q. M. Z. Non-Darcy flow of water-based carbon nanotubes with nonlinear radiation and heat generation/absorption. *Results Phys.* **8**, 473–480 (2018).
28. Chaudhary, M. A. & Merkin, J. H. A simple isothermal model for homogeneous–heterogeneous reactions in boundary-layer flow. I Equal diffusivities. *Fluid Dyn. Res.* **16**, 311–333 (1995).
29. Bhattacharyya, K. Dual solutions in boundary layer stagnation-point flow and mass transfer with chemical reaction past a stretching/shrinking sheet. *Int. Commun. Heat Mass Transf.* **38**, 917–922 (2011).
30. Rashidi, M. M., Rahimzadeh, N., Ferdows, M., Uddin, M. J. & Beg, O. A. Group theory and differential transform analysis of mixed convective heat and mass transfer from a horizontal surface with chemical reaction effects. *Chem. Eng. Commun.* **199**, 1012–1043 (2012).
31. Hayat, T., Hussain, Z., Alsaedi, A. & Mustafa, M. Nanofluid flow through a porous space with convective conditions and heterogeneous–homogeneous reactions. *J. Taiwan Institute Chem. Eng.* **70**, 119–126 (2017).
32. Hussain, Z., Hayat, T., Alsaedi, A. & Ahmed, B. Darcy Forhheimer aspects for CNTs nanofluid past a stretching cylinder; using Keller box method. *Results Phy.* **11**, 801–816 (2018).
33. Lax, F. C. & Kulacki, F. A. The effect of variable viscosity on convective heat transfer along a vertical surface in a saturated porous medium. *J. Heat Mass Transf.* **33**, 10284031 (1990).
34. Crane, J. L. Boundary layer flow on a circular cylinder moving in a fluid at rest. *Zeitschrift für angewandte Mathematik und Physik ZAMP* **23**, 201–212 (1972).
35. Xue, Q. Model for thermal conductivity of carbon nanotube based composites. *Phys. B Condens. Matter* **368**, 302–307 (2005).
36. Babu, M. J. & Sandeep, N. 3D MHD slip flow of a nanofluid over a slendering stretching sheet with thermophoresis and Brownian motion effects. *J. Mol. Liq.* **222**, 1003–1009 (2016).
37. Sreedevi, P., Reddy, P. S. & Chamkha, A. J. Magneto-hydrodynamics heat and mass transfer analysis of single and multi-wall carbon nanotubes over vertical cone with convective boundary condition. *Int. J. Mech. Sci.* **135**, 646–655 (2018).

Author contributions

Mathematical modeling and computational portion of manuscript have been done by Dr. Z.H. The manuscript is proof read and analysis the results by Prof. Dr. T.H. and Prof. Dr. A.A.The newly added author "M.S.A." has substantially help addressing the respected reviewers comments point by point. Furthermore, he has contributed modeling, computation and associated analysis of revised manuscript.

Competing interests

The authors declare no competing interests.

Additional information

Correspondence and requests for materials should be addressed to Z.H.

Reprints and permissions information is available at www.nature.com/reprints.

Publisher's note Springer Nature remains neutral with regard to jurisdictional claims in published maps and institutional affiliations.